mine directly (Eq. 4) (*24*). This change is especially significant genetically in mammalian DNA (*1–6*), whose methylation patterns are critical to gene regulation and differentiation (*25*).

The results show that NO induces a mutation in bacteria that in people has been linked to a variety of disorders suspected to result from base deamination. The list of conditions in which such G:C→A:T transitions have been implicated includes hemophilia (*2*), familial Alzheimer's disease (*3*), colon cancer (*5*), retinoblastoma (*6*), and Gerstmann-Sträussler syndrome (*26*), to name just a few.

Nitrosative deamination of DNA by NO may represent an important mechanism of genomic alteration. Given the numerous sources of human exposure to endogenously as well as exogenously produced nitric oxide (*8–11, 14*), and recent evidence for NO-induced DNA damage in mammalian cell lines (*12, 27*), this pathway's possible involvement in the above-mentioned and other genetic changes thought to arise from deamination of nucleic acids should be well-worth exploring.

REFERENCES AND NOTES

1. M. F. Perutz, *Biophys. Chem.* **37**, 25 (1990); D. N. Cooper and M. Krawczak, *Hum. Genet.* **85**, 55 (1990); R. Hirschhorn, S. Tzall, A. Ellenbogen, *Proc. Natl. Acad. Sci. U.S.A.* **87**, 6171 (1990).
2. J. K. Pattinson *et al.*, *Blood* **76**, 2242 (1990).
3. A. Goate *et al.*, *Nature* **349**, 704 (1991).
4. W. M. Rideout III, G. A. Coetzee, A. F. Olumi, P. A. Jones, *Science* **249**, 1288 (1990).
5. M. Hollstein, D. Sidransky, B. Vogelstein, C. C. Harris, *ibid.* **253**, 49 (1991).
6. D. W. Yandell *et al.*, *N. Engl. J. Med.* **321**, 1689 (1989).
7. L. A. Frederico, T. A. Kunkel, B. R. Shaw, *Biochemistry* **29**, 2532 (1990). The rate for 5-methylcytosine is estimated to be three- to fivefold greater [M. Ehrlich, X.-Y. Zhang, N. M. Inamdar, *Mutat. Res.* **238**, 277 (1990)], whereas purine bases appear to be less reactive than cytosine [R. Shapiro and R. S. Klein, *Biochemistry* **5**, 2358 (1966)].
8. "Oxides of Nitrogen," *WHO Environ. Health Criteria 4* (1977).
9. S. Moncada and E. A. Higgs, *Nitric Oxide from L-Arginine: A Bioregulatory System* (Elsevier/Excerpta Medica, Amsterdam, 1990); J. R. Lancaster, Jr., and J. B. Hibbs, Jr., *Proc. Natl. Acad. Sci. U.S.A.* **87**, 1223 (1990); M. A. Marletta, *Chem. Res. Toxicol.* **1**, 249 (1988); J. Garthwaite, S. L. Charles, R. Chess-Williams, *Nature* **336**, 385 (1988); D. S. Bredt, P. M. Hwang, S. H. Snyder, *ibid.* **347**, 768 (1990).
10. L. J. Ignarro, *Annu. Rev. Pharmacol. Toxicol.* **30**, 535 (1990).
11. Nitrate excretion attributed to NO biosynthesis was found at levels of 1 to 9 mmol/day in people [S. R. Tannenbaum, J. S. Wishnok, C. D. Leaf, *Am. J. Clin. Nutr.* **53**, 247 S (1991)], whereas experiments with mice suggest that immunological stimulation could give up to 200 mmol/day in a 70-kg person [D. J. Stuehr and M. A. Marletta, *Proc. Natl. Acad. Sci. U.S.A.* **82**, 7738 (1985)].
12. T. T. Nguyen, D. C. Brunson, J. S. Wishnok, S. R. Tannenbaum, C. L. Crespi, *Proc. Am. Assoc. Cancer Res.* **32**, abstract 644 (1991).
13. D. A. Wink *et al.*, *ibid.*, abstract 673.
14. D. Ralt, J. S. Wishnok, R. Fitts, S. R. Tannenbaum, *J. Bacteriol.* **170**, 359 (1988); X.-B. Ji and T. C. Hollocher, *Appl. Environ. Microbiol.* **54**, 1791 (1988); H. Kosaka, J. S. Wishnok, M. Miwa, C. D. Leaf, S. R. Tannenbaum, *Carcinogenesis* **10**, 563 (1989).
15. D. L. H. Williams, *Nitrosation* (Cambridge Univ. Press, Cambridge, 1988).
16. H. S. Shapiro and E. Chargaff, *Biochemistry* **5**, 3012 (1966); N. K. Kochetkov and E. I. Budovskii, *Organic Chemistry of Nucleic Acids* (Plenum, London, 1972), p. 362.
17. R. C. Moschel and L. K. Keefer, *Tetrahedron Lett.* **30**, 1467 (1989).
18. B. Singer and D. Grunberger, *Molecular Biology of Mutagens and Carcinogens* (Plenum, New York, 1983).
19. C. M. Maragos *et al.*, *J. Med. Chem.*, in press.
20. D. M. Maron and B. N. Ames, *Mutat. Res.* **113**, 173 (1983).
21. T. A. Cebula and W. H. Koch, *ibid.* **229**, 79 (1990).
22. S. S. Wallace, *Environ. Mol. Mutagen.* **12**, 431 (1988).
23. D. Sagher and B. Strauss, *Biochemistry* **22**, 4518 (1983); L. A. Loeb and K. C. Cheng, *Mutat. Res.* **238**, 297 (1990).
24. This lesion is responsible for certain mutational hotspots in *Escherichia coli* [C. Coulondre, J. H. Miller, P. J. Farabaugh, W. Gilbert, *Nature* **274**, 775 (1978)]; G:T mismatch repair enzymes exist, but are not 100% efficient [T. C. Brown and J. Jiricny, *Cell* **50**, 945 (1987)]. Two of many other mechanisms by which NO might conceivably cause G:C→A:T transitions include deamination of dG (Eq. 5), an apparently nonreparable lesion [T. Lindahl, *Mutat. Res.* **238**, 305 (1990)], and formation of nitrosamine carcinogens [C. D. Leaf, J. S. Wishnok, S. R. Tannenbaum, *Carcinogenesis* **12**, 537 (1991)] that can O^6-methylate guanine [see S. Sukumar, V. Notario, D. Martin-Zanca, M. Barbacid, *Nature* **306**, 658 (1983)].
25. A. P. Feinberg and B. Vogelstein, *Nature* **301**, 89 (1983).
26. K. Hsiao *et al.*, *ibid.* **338**, 342 (1989).
27. T. Nguyen *et al.*, *Proc. Natl. Acad. Sci. U.S.A.*, in press.
28. K. S. Kasprzak, B. A. Diwan, N. Konishi, M. Misra, J. M. Rice, *Carcinogenesis* **11**, 647 (1990).
29. N. Shivapurkar, M. J. Wilson, L. A. Poirier, *ibid.* **5**, 989 (1984).
30. H. Federn and H. Ristow, *Chromatographia* **22**, 287 (1986).

31. Funded in part under NCI contract no. N01-CO-74102.

6 August 1991; accepted 10 October 1991

Prediction of a Crystallization Pathway for Z-DNA Hexanucleotides

P. SHING HO,* TODD F. KAGAWA, KAIHAN TSENG, GARY P. SCHROTH, GUANGWEN ZHOU

Crystallization of macromolecules for structural studies has long been a hit-or-miss process. The crystallization of hexanucleotides as Z-DNA was studied, and it was shown that the cation concentration for crystal formation could be predicted from solvation free energy (SFE) calculations. Solution studies on the conformation and solubilities of the hexanucleotides showed that a critical concentration of the DNA in the Z-conformation must be present in solution to effect crystallization. The SFE calculations therefore predict the propensity of the hexanucleotides to adopt the left-handed conformation and the driving force required to reach this critical concentration relative to the intrinsic solubility of Z-DNA for crystallization.

SINGLE-CRYSTAL STUDIES ON OLIGONUCLEOTIDES have provided a wealth of structural information on the currently recognized forms of DNA and RNA and have the potential to expand our understanding of other important conformations. The general application of x-ray diffraction is limited to cases where diffraction-quality single crystals can be obtained. The "science" of crystal growth has, at best, been a hit-or-miss proposition.

The crystallization of polynucleotides is further complicated by a number of factors. The dense packing of DNA and RNA into a crystal necessarily requires high salt concentrations to counterbalance the negatively charged phosphate backbone. At least for DNA, varying the ionic condition also affects the conformation of the molecule in solution. DNA structures are of interest because of their high degree of polymorphism and because sequence and environment can affect their conformations. These same factors, however, significantly hinder DNA crystallization by introducing a high degree of conformational heterogeneity to the oligomers in solution. In this report, we describe studies that address the critical steps in the crystallization of hexanucleotides as Z-DNA, including the stabilization of the Z-conformation under solutions that are relevant to crystallization and the intrinsic solubility of the Z-conformation at these conditions. From this, a pathway is predicted that allowed us to crystallize the previously unstudied sequence d(CICGCG) as Z-DNA.

In order to gain insight into the factors that stabilize Z-DNA at the molecular level, the structures for a number of hexanucleotides have been studied by x-ray diffraction at atomic resolution (*1*). The crystals of these hexanucleotides are all isomorphous,

Department of Biochemistry and Biophysics, Oregon State University, Corvallis, OR 97331.

*To whom correspondence should be addressed.

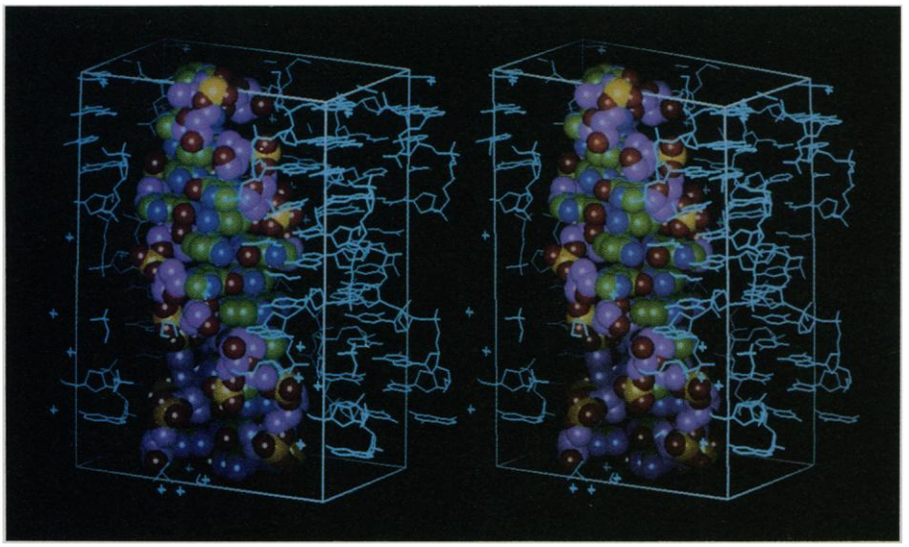

Fig. 1. Stereo diagram of the crystal packing of d(CGCGCG) as Z-DNA. The unit cell typical for hexanucleotides crystallized as Z-DNA in the $P2_12_12_1$ space group is outlined in white. The diagram is slightly extended along the *x*- and *y*-axes to include all of the atoms representing at least two complete hexamers in the crystal (shown represented as van der Waal's spheres). The neighboring hexamers that complete the crystal packing are shown as simple bonds. The hexamers stack end-to-end along the crystallographic *c*-axis to form essentially continuous strands of Z-DNA.

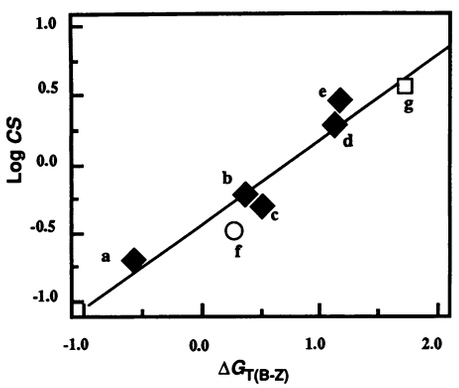

Fig. 2. Plot of cation strength (*CS*) at which Z-DNA hexamers crystallized versus B- to Z-DNA transition energies ($\Delta G_{T(B\text{-}Z)}$) predicted from SFE calculations. Data for the previously crystallized hexamers from other laboratories are plotted as filled diamonds: (a) d($m^5CG)_3$ (*8*); (b) d(CDCGTG) (*6*); (c) d(m^5CGTAm^5CG) (*9*); (d) $d(CG)_3$ (*10*); and (e) d(CACGTG) (*11*). Sequences crystallized in this laboratory are plotted as an open circle [(f), d(m^5CGUAm^5CG)] (*5*) and as an open square [(g), d(CICGCG)] from this study. The linear regression fit of the points yields a relation of $\log(CS) = 0.66\Delta G_{T(B\text{-}Z)} - 0.40$. The standard error of the slope is 0.09 and of the intercept is 0.08.

which suggests that the crystal packing is specific for this length and conformation of the DNA (Fig. 1). In general, such crystals are obtained by the vapor diffusion method in which the DNA, a buffer, various salts, and a precipitant (2-methyl-2,4-pentanediol or MPD) in a crystallization well are allowed to equilibrate against a large reservoir of a higher concentration precipitant solution under a closed system. Upon equilibration, the crystallization solution is concentrated until the DNA is no longer soluble so that it forms either an amorphous precipitate or an ordered array.

A broad spectrum of salt and buffer concentrations (typically up to 1.5 M) is normally searched when attempting to crystallize a new hexamer sequence as Z-DNA. Since cations affect the stability of Z-DNA more so than do anions, the general ionic environment at any stage of the crystallization can be described by a cation strength (*CS*) (*2*). The precipitant concentration (typically 35 to 50% MPD, v:v) affects the solubility and, to some extent, the stability of Z-DNA. A number of multivalent polyamines and metal complexes have facilitated the crystallization of some hexamers. All of these factors affect the relative stability of Z-DNA, which suggests that the crystallization of hexanucleotides as Z-DNA is dependent on the ability of the sequence to adopt the Z-conformation. The two factors, therefore, that need to be considered in crystallizing Z-DNA are (i) the stabilization of the conformation in solution and (ii) the solubility of the DNA under these conditions.

We studied the relative stability of B- versus Z-DNA by calculating the solvent free energy (SFE) difference between the two DNA forms (*2*). The effects of methylation (*2*) and sequence (*3, 4*) on Z-DNA stability were attributed to the interactions of water with the B- versus the Z-forms. Substituent groups that stabilized Z-DNA were found to increase the hydrophilicity of the solvent-accessible surface of this conformation. The SFE calculations are consistent with the experimentally determined stability of various sequences as Z-DNA in solution (*3*) and the interactions of solvent with Z-DNA observed in single crystals (*5*).

We observed an empirical relation between the cation strengths reported for the crystallization of hexanucleotides as Z-DNA versus the SFE predictions for the ability of these sequences to adopt the Z-conformation (Fig. 2). The SFE calculations do not take into account the components of the crystallization solutions and therefore do not directly estimate the stability of the hexamer sequences as Z-DNA under the crystallization conditions. They do, however, estimate the propensity of a sequence to adopt the Z-conformation and thus predict the effect of sequence on the driving force (the CS and MPD in the crystallization solutions) required to induce a B- to Z-DNA transition. Therefore, Fig. 2 relates the driving force for inducing Z-DNA in the crystallization solution to the propensity for the sequence to adopt the Z-conformation. This relation also holds for the crystallization of sequences containing unnatural bases, including deoxyuridine bases, as in the sequence d(m^5CGUAm^5CG) crystallized by Zhou and Ho (*5*), and diaminoadenine (D) bases, as in d(CDCGTG) crystallized by Coll *et al.* (*6*). In both cases, the cation strengths required for crystallization were consistent with their predicted stabilities as Z-DNA.

In this study we used the SFE calculations to actually predict a target cation strength for crystallizing the previously unstudied sequence d(CICGCG) as Z-DNA. The SFE calculations indicated that deaminating guanine bases at the N2 position destabilizes Z-DNA by +0.28 kcal/mol per base pair (*4*), so that the propensity for d(CI) to adopt the Z-conformation is lower than even d(TA). The crystallization of d(CICGCG) would therefore require a significantly higher *CS* (4.2 M) than that for any previous alternating pyrimidine-purine hexanucleotide. We used this prediction to set up a crystallization experiment for d(CICGCG) as listed in Table 1. The cation strengths upon equilibration against 30% MPD were lower than the targeted *CS* = 4.2 M in all six wells. Under these conditions, the DNA in wells 1 and 2 and in wells 4 and 5 precipitated as amorphous oils that eventually became highly disordered crystals. These crystals could not be indexed for diffraction studies; we therefore did not pursue this route as a general strategy for crystallizing Z-DNA hexanucleotides and, instead, focused on direct crystallizations from solution. The solutions in wells 3 and 6 remained clear after equilibration at 30% MPD.

The salts in the crystallization wells increase upon equilibration against 50% MPD such that only well 3 reaches the target cation strength. Within 1 week, a single large diffraction-quality crystal, which was isomorphous with previous Z-DNA crystals, was obtained in well 3. A cluster of Z-DNA–like crystals also grew in well 6. Smaller, Z-DNA–like crystals were also observed in well 2, while only amorphous precipitates were observed for wells 1, 4, and 5. Thus, the hexanucleotide sequence d(CICGCG) crystallizes as Z-DNA at the target conditions predicted from the SFE calculations. The predicted crystallization pathway falls in a narrow range of cation strengths (2.8 to 4.2 M) that yield Z-DNA crystals. This path, although not unique, avoids precipitation and therefore maintains sufficient quantities of the hexanucleotide in solution to undergo a B- to Z-DNA transition. The question, then, is what do the SFE calculations actually predict in terms of Z-DNA crystallization?

The concentration of d(CICGCG) hexamer remaining in well 3 after crystal growth was determined to be 0.21 mM, or an intrinsic solubility (S^0) for the d(CICGCG) crystals of 8.2×10^{-4} (7). When compared to other hexanucleotide sequences (Table 2), S^0 of the Z-DNA crystals appear to mirror the differences in SFE for the Z- versus the B-conformations. The intrinsic solubilities are therefore dependent on the propensity of the hexanucleotide to adopt the Z-conformation. This finding is consistent with the premise of the SFE calculations that sequences which are more stable as Z-DNA are more hydrophilic than sequences that are not as stable. The order of magnitude of the S^0 values, however, is significantly greater than the variation over these values, suggesting that there is an overall intrinsic solubility for the hexamer. Thus, there is a critical concentration of DNA for Z-DNA crystallization. Must the DNA at this critical concentration, however, be in the Z-conformation?

The conformations of d(CICGCG) were studied spectroscopically at cation strengths and MPD concentrations that mimic the crystallization process (Fig. 3). The ultraviolet (UV) absorption spectra at $CS \leq 2.3$ M, 0% MPD was essentially that of single-stranded DNA. The spectra collapsed to that of duplex B-DNA at $CS = 4.2$ M, 0% MPD and at $CS = 2.3$ M, 10% MPD. At the initial phases of the crystallization process, therefore, the hexanucleotide undergoes a single-stranded to B-DNA transition. Furthermore, MPD appears to stabilize the duplex conformations of DNA.

At MPD concentrations ≥35%, the ultraviolet absorption spectra become sharper and the absorbance maxima (A_{max}) shift to longer wavelengths (Fig. 3C). At 35% MPD and at all cation strengths, the spectra were identical ($A_{max} = 268$ nm). The 15% hypochromism as CS increased from 0 to 4.2 M is consistent with a salt-induced single-stranded to duplex DNA transition. The circular dichroism (CD) spectra of the hexanucleotides at $CS \geq 2.3$ M, 35% MPD are typical of a right-handed B-DNA.

The spectra at $CS \leq 2.3$ M, 50% MPD (Fig. 3D) were nearly identical in shape and overall absorbance to those at 35% MPD, but A_{max} at $CS = 4.2$ M was shifted to 272 nm. The $CS = 4.2$ M minus $CS = 2.3$ M difference spectrum showed a maximum positive absorbance at 292 nm and a minimum negative absorbance at ~260 nm and was characteristic of a solution of ~60%

Table 1. Crystallization of d(CICGCG) as Z-DNA. Listed are the cation strengths (CS) and the state of the DNA at the initial MPD concentrations and after equilibration against 30% and 50% MPD in the reservoir. The initial MPD concentrations were 10% for wells 1, 2, and 3 and 15% for wells 4, 5, and 6. Cation strength was calculated as $CS = [Na^+] + 4[Mg^{2+}]$, where $[Na^+]$ is the concentration of the sodium cation in the sodium cacodylate buffer and $[Mg^{2+}]$ is the concentration of magnesium chloride in solution. These were calculated under initial conditions and after equilibration against 30% and 50% MPD in the reservoir of the crystallization setups. For the DNA, P refers to the observed amorphous precipitate or disordered crystals in the crystallization well, C refers to diffraction quality Z-DNA crystals, and S refers to the DNA remaining in solution with no observed precipitates or crystals.

Well (no.)	Initial CS	30% MPD		50% MPD	
		CS	DNA	CS	DNA
1	0.43	1.30	P	2.17	P
2	0.63	1.90	P	3.17	P, C
3	0.83	2.50	S	4.17	C
4	0.43	0.87	P	1.44	P
5	0.63	1.27	P	2.11	P
6	0.83	1.67	S	2.78	C

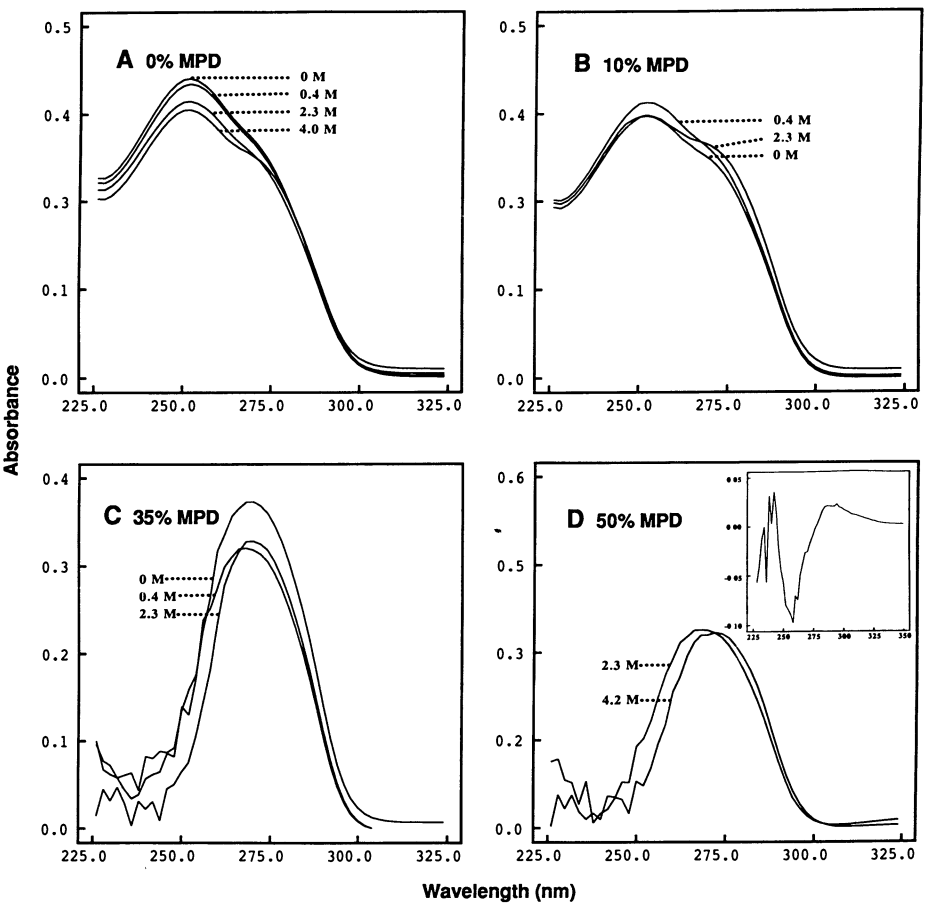

Fig. 3. Ultraviolet absorption spectra of d(CICGCG) at different MPD concentrations and CS. (**A**) Spectra at 0% MPD for $CS = 0.0$, 0.43, 2.3, and 4.2 M, with the absorbance maximum (A_{max}) at 256 nm. (**B**) Spectra at 10% MPD for $CS = 0.0$, 0.43, 2.3, and 4.2 M. (**C**) Spectra at 35% MPD ($A_{max} = 268$ nm). The spectra for $CS = 0.0$, 0.43, and 2.3 M are shown. The $CS = 4.2$ M spectrum, which is nearly identical to that of $CS = 2.3$ M, is omitted for clarity. (**D**) Comparison of spectra at $CS = 2.3$ ($A_{max} = 268$ nm) versus 4.2 M ($A_{max} = 272$ nm), at 50% MPD. Spectra at $CS = 0.0$ and 0.43 M, 50% MPD are nearly identical to that of $CS = 2.3$ M. The inset shows the difference spectrum of $CS = 4.2$ M minus $CS = 2.3$ M at 50% MPD.

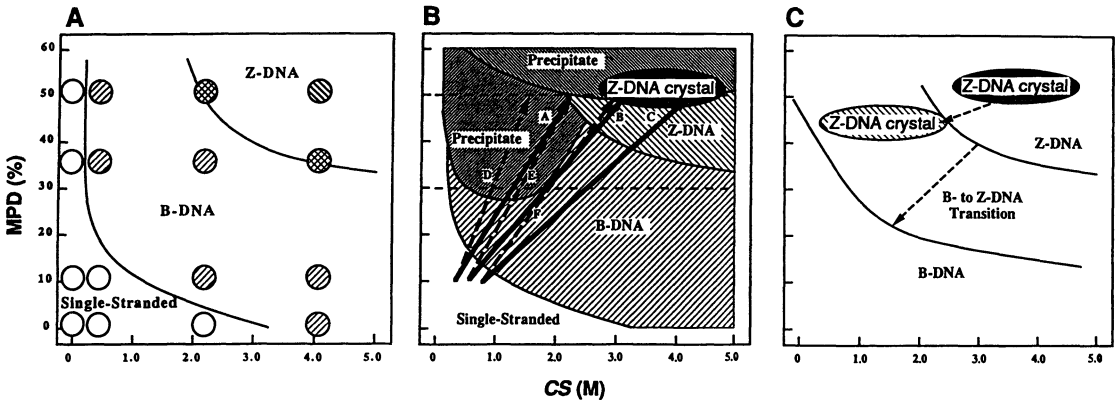

Fig. 4. Cation strength versus MPD phase diagram for crystallization solutions of d(CICGCG) as Z-DNA. (**A**) Conformations from UV absorption and CD studies on d(CICGCG). Open circles represent single-stranded DNA, right-hashed circles represent duplex (presumably B-form) DNA, and the left-hashed circle represents predominantly Z-DNA in solution. Circles that are both right- and left-hashed represent near equal mixtures of B- and Z-DNA according to CD studies. The transition interfaces for the three conformations are delineated. (**B**) Phase diagram for the solution and precipitated forms of d(CICGCG), as labeled. The vectors A to C (solid arrows) represent crystallization pathways for crystallization wells 1, 2, and 3, respectively. Similarly, vectors D to F (broken arrows) represent pathways in wells 4, 5, and 6, respectively. (**C**) Effect of Z-DNA stability on the phase diagram for crystallization of hexanucleotides. The broken arrows indicate the nearly parallel shift to lower *CS* and MPD concentrations for the B- to Z-DNA transition (curve) and the Z-DNA crystal domain (hashed oval) as the propensity of a sequence to adopt the Z-conformation increases.

Table 2. Comparison of the intrinsic solubilities (S^0) of Z-DNA hexamer crystals versus the difference in solvent free energy between Z- to B-DNA transition [$\Delta SFE_{(Z\text{-}B)}$], as calculated from solvent accessible surfaces.

Sequence	S^0 ($\times 10^3$)	$\Delta SFE_{(Z\text{-}B)}$ (kcal/mol)
d(m^{5}CGUAm^{5}CG)	3.1	−0.221
d(m^{5}CGTAm^{5}CG)	2.1	−0.099
d(CG)$_3$	0.98	0.216
d(CICGCG)	0.82	0.482

Z-DNA. This result was confirmed by the CD spectrum. Thus, d(CICGCG) is predominantly in the Z-form under conditions that the SFE calculations predict would stabilize Z-DNA and yield Z-DNA crystals. Under all other solution conditions, the DNA was either single-stranded or in the B-form. The CD studies also suggested that some Z-DNA was present at *CS* = 2.0 M, 50% MPD and *CS* = 4.2 M, 35% MPD. The crystallization of hexanucleotides as Z-DNA therefore requires a critical concentration of the left-handed Z-conformation. Furthermore, the conditions, particularly the cation strength, at which this critical concentration occurs can be predicted by the SFE calculations.

Mapping these conformations on a CS versus MPD plot results in a phase diagram for d(CICGCG) under the solution conditions that are relevant for its crystallization (Fig. 4A). This diagram shows the solution conditions that stabilize the various conformations of the hexanucleotide. When the observations from the actual crystallization of the sequence are taken into account, the solution phases can be related to the nonsolution phases of the hexanucleotide (Fig. 4B). The crystallization paths for the conditions in Table 1 are represented as vectors A to C for wells 1 to 3 (solid arrows) and D to F for wells 4 to 6 (dashed arrows). An interface between B-DNA in solution and a precipitate is defined near 30% MPD at *CS* < 2.0 M, as indicated by the observed precipitates in wells 1 and 2. The eventual formation of Z-DNA–like crystals in well 2 at 50% MPD suggests that the edge of this interface lies along the crystallization vector B. Vector C traces the DNA transitions within well 3 during crystallization. The narrow Z-DNA crystal domain shown lying between vectors B and C is a minimum range for this phase.

The effect of sequence on the domains of the phase diagram is shown in Fig. 4C. As the propensity for a sequence to adopt the Z-conformation increases, the driving force (the salt and MPD) required to induce the B- to Z-DNA transition in solution decreases. There is an intrinsic solubility of the hexanucleotide as Z-DNA that defines a critical concentration for its crystallization. Thus, as the B- to Z-DNA transition in solution shifts to lower salt and MPD concentrations, the crystalline Z-DNA domain shifts along a nearly parallel path. The SFE calculations therefore predict the propensity for the hexanucleotides to adopt the Z-conformation and thus the placement of the B- to Z-DNA transition interface and the Z-DNA crystal domain within the phase diagram for crystallization for a given hexanucleotide sequence.

These studies show that, with sufficient knowledge of a DNA system in terms of conformational stability and solubilities, we could predict a path that led to precipitation of a particular conformation of an oligonucleotide. In this case, we relied on the intermolecular packing forces to precipitate Z-DNA hexamers as a crystal. The nature of these forces and why they appear to be unique for hexanucleotides are not fully understood; however, knowing that they exist, we can predict how to crystallize a hexamer sequence as Z-DNA. Thus macromolecular crystallization, at least for oligonucleotides, can be approached in a systematic manner. In order to apply this to the crystallization of different lengths and conformations of DNA (such as B-DNA), a similar set of phase diagrams relating conformational stability and solubility would need to be developed. Once understood, however, the relation between the stability and intrinsic solubilities of polynucleotide conformations could be exploited to develop rational approaches to the crystallization of novel and interesting DNA and RNA molecules for structural studies.

REFERENCES AND NOTES

1. T. M. Jovin, D. M. Soumpasis, L. P. McIntosh, *Annu. Rev. Phys. Chem.* **38**, 521 (1987).
2. P. S. Ho, G. J. Quigley, R. Tilton, A. Rich, *J. Phys. Chem.* **92**, 939 (1988).
3. T. Kagawa, D. Stoddard, G. Zhou, P. S. Ho, *Biochemistry* **28**, 6642 (1989).
4. K. Tseng and P. S. Ho, unpublished results.
5. G. Zhou and P. S. Ho, *Biochemistry* **29**, 7229 (1990).
6. M. Coll, A. H. J. Wang, G. A. van der Marel, J. H. van Boom, A. Rich, *J. Biomol. Struct. Dyn.* **4**, 157 (1986).
7. Intrinsic solubility is defined as S^0 = [DNA$_s$]/[DNA$_c$], where [DNA$_s$] is the concentration of the DNA in solution and [DNA$_c$] is the concentration of DNA in the crystal. [DNA$_c$] was estimated from the packing of four hexamer duplexes in a volume of ~26,000 Å^3 to be 0.26 M.
8. S. Fujii, A. H.-J. Wang, G. A. van der Marel, J. van Boom, A. Rich, *Nucleic Acids Res.* **10**, 7879 (1982).
9. A. H. J. Wang, T. Hakoshima, G. A. van der Marel, J. H. van Boom, A. Rich, *Cell* **37**, 321 (1984).
10. A. H. J. Wang *et al.*, *Nature* **282**, 680 (1979).
11. M. Coll *et al.*, *Nucleic Acids Res.* **16**, 8695 (1988).

12. Supported by the Office of Naval Research (contract no. N00014-88-K-0388) and the American Cancer Society (grant no. NP740). P.S.H. is a recipient of a Junior Faculty Research Award from the American Cancer Society (JFRA no. 306).

4 June 1991; accepted 12 August 1991